

5YSZ Powders from Gels: Densification and Microstructure Characterization

Carmen Barrera-Solano, Luis Esquivias* and Manuel Piñero

Departamento de Física de la Materia Condensada, Facultad de Ciencias, Universidad de Cádiz, Apartado 40, Puerto Real, 11510 Cádiz, Spain

(Received 28 July 1997; accepted 19 December 1997)

Abstract

Five mol% yttria doped zirconia powders were prepared by controlled hydrolysis of alkoxides. Their sintering behavior was monitored by dilatometry to optimize the sintering schedule. The compact bodies were characterized by SEM and quantitative analysis of their X-ray patterns. Re-sintering under axial pressure slightly improved the final relative density of the zirconia powders at the expense of a grain size increase that, however, for most of them remains submicrometric. © 1998 Elsevier Science Limited. All rights reserved

1 Introduction

Hydrolysis and polycondensation of alkoxides¹ constitute an alternative method to obtain very pure and easily sinterable powders, once a total elimination of the unwanted organic residues has been completed. This method allows controlling the important powders characteristics such as particle size and size distribution, form and agglomeration.² This technique is attractive for ceramics powders production because which reaction are fast (seconds or few minutes) with a high yield. The alkoxide route for ceramics from gels is very popular because the procedure stabilizes the element in its higher oxidation state as a consequence of the presence of the -OR group. However, commercial alkoxides are expensive and sometimes difficult to find. Thus, only an optimum performance of the products from powders prepared by this method would make advisable its use.³

We have shown, contrary to what happens in the powders prepared by coprecipitation,⁴ that controlled hydrolysis of alkoxides allows the preparation

of zirconia–yttria solid solution in which Y atoms are in the ZrO₂ lattice from the very beginning of the process.⁵ In the crystallized powders, the homogeneity is much higher than the powder described in Ref. 4. This agrees with the reported characteristic of the sol–gel processing, i.e. this technique guarantees homogeneity at a molecular level. We found this result interesting enough to initiate a study on the sintering behavior and mechanical performance of bulks prepared from these powders.

The strength of a ceramic prepared by free sintering depends on the defects of the green compact⁶ which causes different rate of sintering in distinct areas of the powder compact. This gives rise to strain gradients these in turn generate internal stresses which opposes the sintering pressure and inhibit sintering. Only plastic deformation can relax them. If plastic deformation is faster than densification, then the geometric constraints are unimportant, but if it is slower, internal stresses can arise on block densification and may lead to processing flaws. Hot isostatic pressing and superplastic forging are all techniques which can eliminate flaws arising from packing defects, thereby enhancing the strength and reliability of ceramics. Hot pressing and sinter-forging are somewhat superior in that they stimulate large deviatoric, rather than hydrostatic, stresses and strains and hence stimulate a lot of macroscopic plastic flow. In superplastic forging, a presintered sample is submitted to an uniaxial pressure at high temperature. The process is similar to uniaxial hot pressing but unlike the former methods the sample can expand laterally. Venkatachari and Raj^{7,8} studied the performance of superplastic forging to eliminate the processing flaws produced during free sintering of alumina, checking the change in morphology and the frequency of processing flaws after superplastic deformation. They reported an

*To whom correspondence should be addressed.

increase in strength due to strain-controlled healing of sintering flaws. It was also shown that at 20% strain a beginning of an increase in the ceramic's strength could be measured.

In the present work the sintering schedule of five mol% of yttria doped zirconia powders obtained by hydrolysis and polycondensation of alkoxides was optimized by dilatometry. The samples that presented the highest density were subsequently resintered under axial pressure. The microstructure and atomic structure changes caused by resintering were studied by scanning electron microscopy (SEM) and Rietveld analysis.

2 Experimental

Five mol% yttria doped zirconia powders (from now on referred as 5YSZ) obtained by controlled hydrolysis and polycondensation of the appropriate amounts of alkoxide of zirconium *n*-propoxide and yttrium isopropoxide.

An alkoxide controlled hydrolysis method, based in the Fegley and Barringer technique¹⁻³ has been used, with minor changes, in the way described below. As large volumes are required because of the high dilution of the precursors (0.080 M of zirconium propoxide and 0.008 M of yttrium i-propoxide, appropriated to obtain 5 mol% yttria doped zirconia) an inert atmosphere working device has been installed to prepare large amounts of powders. It permits to work with up to 10 volumes of 200 ml with a yield of 75%. The line is connected to a vacuum pump and a nitrogen tank. A valve device allows, alternatively, the inlet or outlet from each of the matrasses. These are isolated from the external atmosphere by means of hermetic stoppers. A vacuum trap preserves the rotatory pump from unwanted liquids and a Hg manometer warns about the nitrogen pressure in the line.

Hydrolysis reactions take place at room temperature in dry atmosphere. The powder was extracted from the solution by centrifugation, then subjected to a washing cyclic process (three times) in distilled water and ethanol consisting of a redispersion by ultrasounds, from a sonifier (KONTES) operating at 20 kHz, with a power output of 16 w. Next, these powders were redispersed ultrasonically in distilled water at pH=10.2. Finally, the powder was settled during several days and the supernatant liquid was taken off and the wet powder was dried in a oven at 40°C. Once dried, the powder was subjected to an oxidation treatment in air at 350°C for 15 h, followed by calcination at 800°C for 2 h.

Several techniques were used to characterize powders. The specific surface area was determined

using nitrogen adsorption by the Brunauer-Emmett-Teller (BET) method were applied to calculate the mean diameter of the powders crystallites, d_{BET} , using the relation assuming spherical or cubic shape of the particles:

$$d_{BET} = \frac{6}{\rho \cdot S} \quad (1)$$

where ρ is the theoretical density, and S is the specific surface area.

The particle size and degree of agglomeration were examined using SEM (JEOL JSM 820). The calcined powders were dispersed in acetone by ultrasonic radiation and placed on a carbon film for this examination. The features of the microstructures were determined with an image analyser (Zeiss Kontro Videoplan).

The crystalline phases were studied by whole profile fitting (WPF) method of X-ray diffraction (XRD) patterns. They were obtained (PHILIPS PW 1830) with Cu $k_{\alpha 1}$ and Cu $k_{\alpha 2}$ radiation ($\lambda_1 = 0.1541$ nm and $\lambda_2 = 0.1544$ nm, respectively) selected by means of graphite monochromator situated after the sample. The working conditions were 40 mA and 40 kV. Data were collected in the interval $10^\circ < 2\theta < 90^\circ$ with a step size of $\Delta(2\theta) = 0.015^\circ$. Counts were measured by keeping a collection time of 1 s step⁻¹.

The data fitting was carried out by means of the FULLPROF⁹ software. This program allows the multiphase analysis of diffraction spectra using the space group and network parameters of the involved phases as starting structural information. The line profile is achieved applying the Marquardt algorithm¹⁰ which minimizes the full width half-maximum intensity (FWHM) of a previously selected analytical function. Silicon was used a reference because of its monophase structure with diffraction peaks near from the zirconia peaks. The 2θ dependence of the FWHM is defined by the usual Cagliotti parameters, U , V and W for the Gaussian contribution and X and Y for the Lorentzian contribution. No free yttria traces were noticed. The profile agreement indices observed for the Pattern-Fitting analysis ranged from 17–23% for R_{WP} , 1.3–4.0% for R_B and 1.4–2.1 for the GofF (goodness of fitting). These factors correspond to the least-square method fitting in the FULLPROF program.¹¹

The diagrams were fitted using space groups; $P4_2/nmc$ for the transformable tetragonal (*t*-ZrO₂) and non-transformable tetragonal (*t'*-ZrO₂) phases, $P21/c$ for monoclinic (*m*-ZrO₂) phase and $Fm\bar{3}m$ for the cubic (*c*-ZrO₂) phase, respectively, using as reticular constant starting values and space group those described in the literature.¹²⁻¹⁴ The same

atomic positions were used for both tetragonal phases.

A Thomson–Cox–Hasting pseudo–Voigt¹⁵ function was used for the profile line fitting. This type of function is suitable because it allows one to determine independently the Gaussian and Lorentzian contributions which are related, respectively, to the average particle size and microstrain. The width in the half maximum (H) of both components are given by

$$H_{k-G} = V \cdot \tan \theta \quad (2)$$

$$H_{k-L} = \frac{X}{\cos \theta} \quad (3)$$

where V and X are parameters obtained from the diffraction profile fitting of the sample.

The average size particle estimate, $\langle p \rangle$, can be achieved applying the expression

$$\langle p \rangle = \frac{180K\lambda}{\pi(X - X_0)} \quad (4)$$

with K being the Scherrer constant, X being the contribution to the integral width due to the grain size and X_0 the same profile parameter of a well-known compound used as a reference. This procedure works when X and X_0 are very different. This is the case for powders but not for the sintered bodies. The relative fraction of the phases present in each sample was evaluated from scale factor refining.¹⁶

Green compact parallelepipeds of ~ 3 mm height and 15×3 mm² base were made for dilatometry experiments (Dilatronic1700 THETA dilatometer equipped with a Dilaflex2 sensor). The as-calcined powders were cold uniaxially pressed under 75 MPa in an appropriate die. These compaction experiments were performed in air, in which the thermocouple is in contact with the sample. Table 1

Table 1. Heat-treatment schedule and codes of the dilatometry experiments on green samples

Code	Heating rate (°C h ⁻¹)	Final temperature (°C)	Dwell time (h)	Relative density (%)
C1	300	1600	0.5	94
C2	600	1600	0.5	94
C3	300 (up to 1250°C) 60 (up to 1550°C)	1550	10	95
C4	300 (up to 1100°C) 60 (up to 1600°C)	1600	0.5	96
C5	300 (up to 1100°C) 60 (up to 1400°C)	1400	10	96
C6	300 (up to 1250°C) 60 (up to 1550°C)	1550	2	96

$$\rho_{\text{theoretical}} = 6.03 \text{ g cm}^{-3}$$

abridges the applied heat-treatments as well as the assigned codes.

Porosity of calcined powders and green samples was characterized by mercury porosimetry (Pascal 440 Fisons Instruments) inside cold uniaxially pressed pellets (75 MPa). The open porosity could thus be quantified.

Cylindrical pellets of ~ 1 cm height and 1.3 cm diameter, were obtained from as-calcined powders cold uniaxially pressed at 75 MPa. The densities of the 'green' compacts were $\sim 39\%$ of theoretical. The density measurements were made using a weight/mensuration technique on the cylindrical coupons after compaction. For the sintering experiments the temperature was raised at a rate of 1°C min to 1400°C. At this temperature the compact was sintered for 2 h in air. The overall densities of the sintered pellets was determined using Archimedes technique (in water). The relative densities were calculated taking 6.03 g cm⁻³ as theoretical density.¹⁷

The microstructure of the pressed samples and the morphology, grain size distribution and grain growth of sintered bodies were examined by SEM. Previously, the sintered bodies were polished and thermally etched in air at 1300°C.

The sintered bodies (cylindric-shaped bodies ~ 9 mm diameter and ~ 6 mm height) were resintered by hot uniaxial pressing in air in an Instron 1185 machine. The temperature of the furnace was increased from room temperature to 1300 or 1400°C at 300°C h⁻¹ heating rate. In order to hold the load constant (20–30 N) during heat-up, the crosshead speed was continuously modified with the aim of compensating the increase of pressure due to the thermal dilatation of the sample. Once the the working temperature was attained and the system stabilized, the compression was commenced after waiting 30 min for stabilization. We assume no shrinkage during equilibration. Three crosshead speeds were used: 5, 20 and 50 $\mu\text{m min}^{-1}$. The axial strain and load were measured continuously with time.

3 Results and Discussion

3.1 Powder characterization

The calcined powder at 800°C (5YSZ800) is weakly agglomerated into 15–300 μm coarse clusters. Scanning electron micrograph of 5YSZ800 powders (Fig. 1) reveals the calcined powder is constituted by near spherical particles. The average form factor is 0.93 (Fig. 2), ranging in size from 80 to 350 nm, with an average particle size of approximately 180 nm (Fig. 3).

Figure 4 shows the Hg intrusion porosimetry results of 5YSZ800 powders. Generally, two different

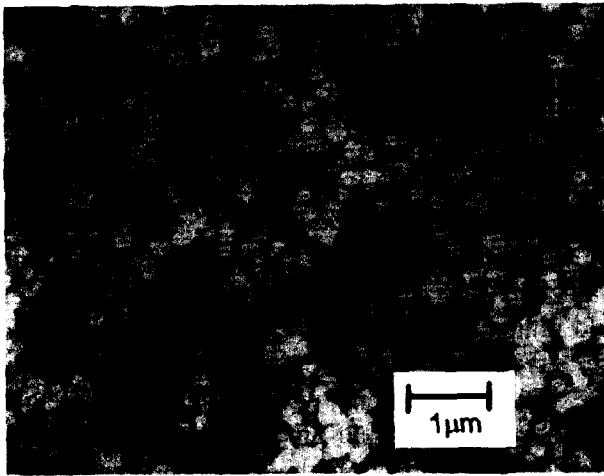


Fig. 1. Scanning electron micrograph of 5YSZ800 powders.

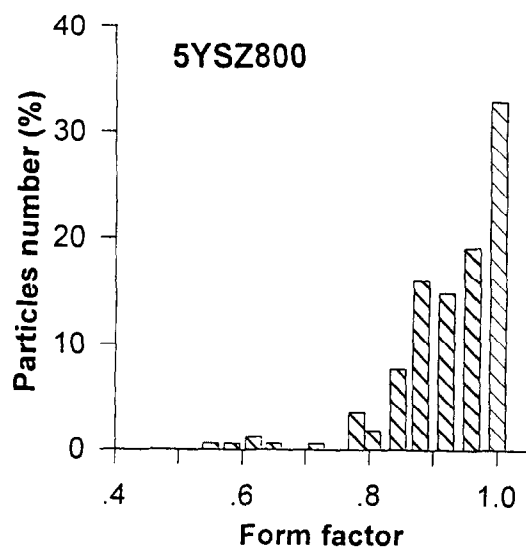


Fig. 2. Form factor of 5YSZ800 powders.

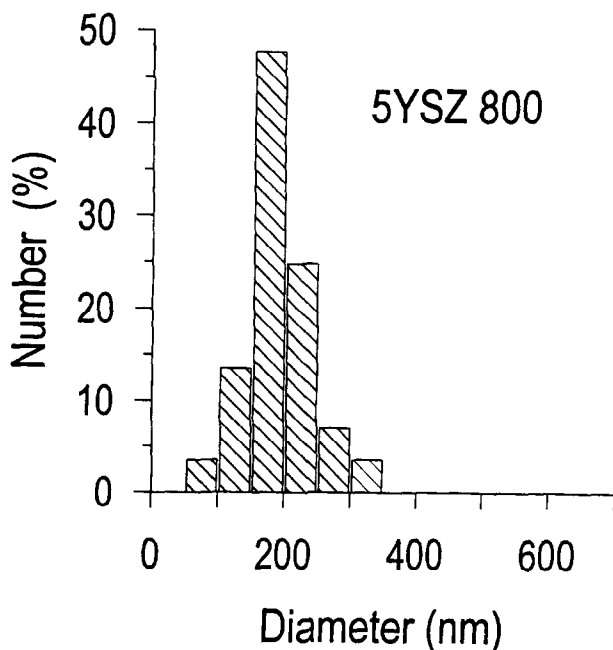


Fig. 3. Particle size distribution of 5YSZ800 powders.

sized pore populations are observed: (1) small, inter-agglomerate pores, fluctuating between 60 and 1000 nm, with a maximum about 200 nm and (2) large, intra-agglomerated pores, in the range 2×10^3 – 6×10^4 nm, with a maximum about 3×10^4 nm.

Standard X-ray diffraction patterns of the powders both as-prepared and treated at temperatures lower than 400°C did not show traces of crystallinity. However, the typical oscillations of the diffracted intensities from amorphous materials are clearly sharper after this heat-treatment (Fig. 5). The WPF refining output plots of the 5YSZ800 powders are shown in Fig. 6. The best results of profile agreement indices were observed when the

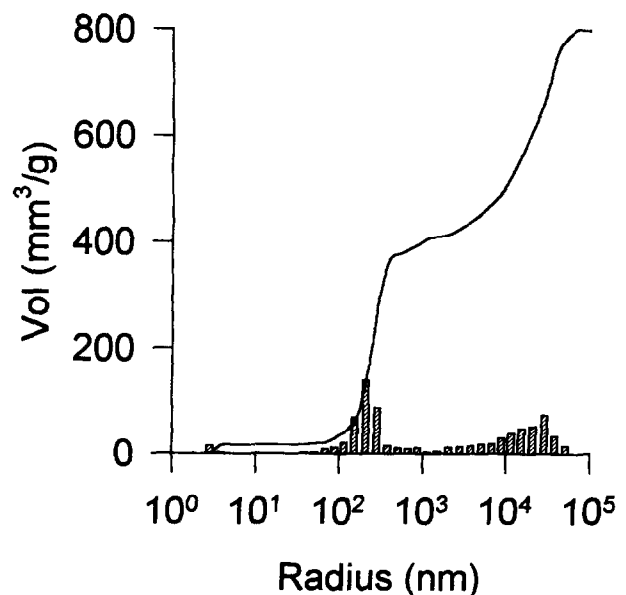


Fig. 4. Pore size distribution (determined by mercury intrusion) of 5YSZ800 powders. Continuous line represents the cumulative volume.

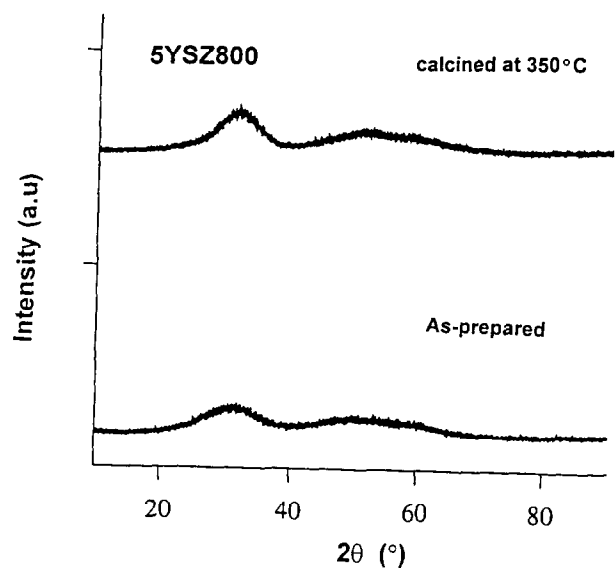


Fig. 5. X-ray diffraction spectra of the powder: (a) as-prepared and (b) treated at 350°C.

t-ZrO₂, t'-ZrO₂, m-ZrO₂ and c-ZrO₂ phases were included in the refinement. Table 2 shows the data obtained from the pattern-fitting analysis and the results of the quantitative analysis data.

The values of the crystallite size, d_X , shown in Table 3, has been calculated from the weighted average of the medium size of each one present phases in the sample.

The difference in crystallite size value found from X-ray diffraction pattern and from S_{BET} can be explained by the fact that in these types of powder the primary crystallites are clustered forming aggregates. In this way nitrogen, used for the BET measurements, cannot completely cover the crystallite surface. So these differences between d_{BET} and d_X give some indication of the degree of aggregation. The basic characteristics of the calcined powder are given in Table 3.

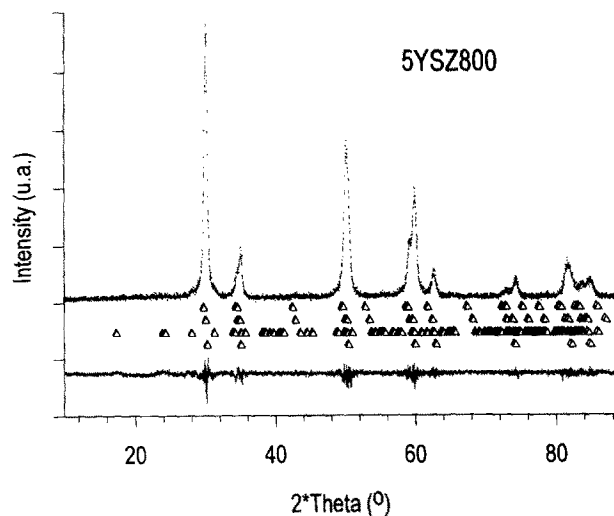


Fig. 6. WPF plots for diffraction data collected from 5YSZ800 powders. The experimental data is indicated by small dots and the calculated patterns by the solid line overlying them. Bars underneath the pattern show the calculated Bragg reflection corresponding to the different phases in the same order that they appear in the respective table. The line at the bottom of the pattern is the difference between the experimental and the calculated profiles.

Table 2. Refinement data, crystallite size and phase composition (wt%) obtained for 5YSZ800 samples

Phase	X	d_X (nm)	wt%
t-ZrO ₂	0.276	35	15
t'-ZrO ₂	0.307	31	8
m-ZrO ₂	0.329	27	47
c-ZrO ₂	0.106	103	30

Table 3. Characteristics of the calcined powders (5YSZ800)

Sample	S_{BET} (m ² g ⁻¹)	d_{BET} (nm)	d_X (nm)	Relative density (%)
5YSZ800	14	72	68	14

$$\rho_{\text{theoretical}} = 6.03 \text{ g cm}^{-3}$$

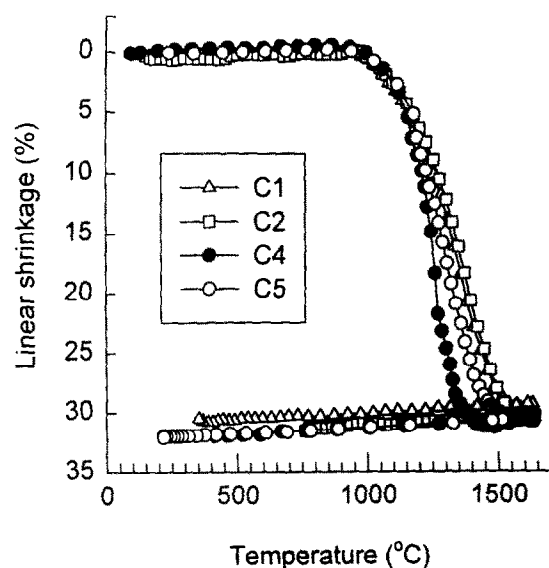
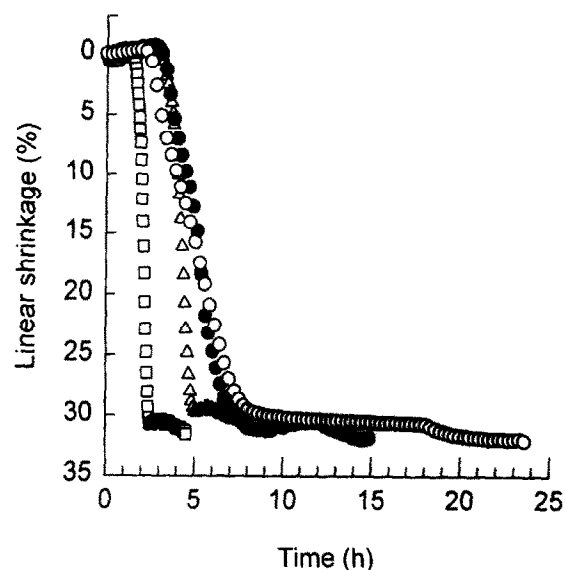


Fig. 7. Shrinkage behavior of the specimens during sintering versus time (above) and temperature (below) for the sintering schedules shown in Table 2.

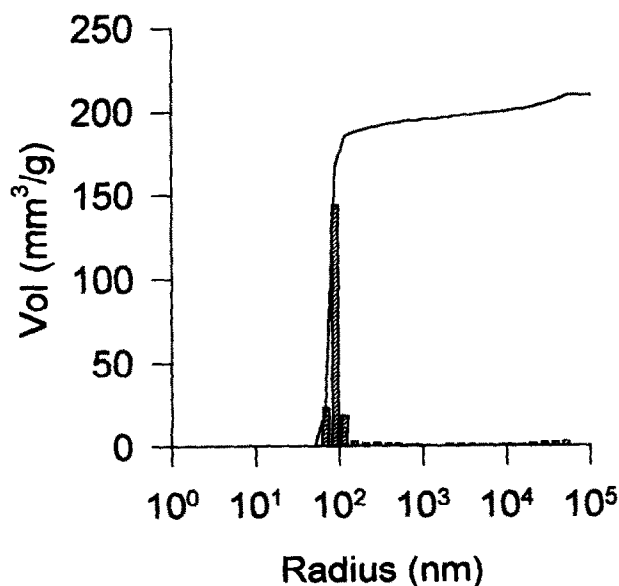


Fig. 8. Pore size distribution (determined by mercury intrusion) of the green bodies. Continuous line represents the cumulative volume.

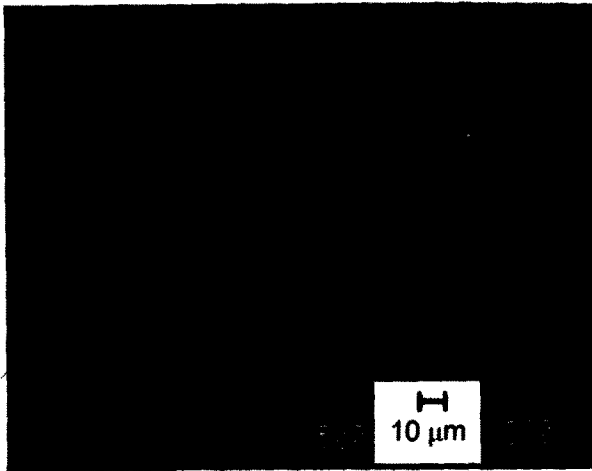


Fig. 9. Scanning electron micrograph of fractured surfaces of green body uniaxially compacted up to 75 MPa (Bar = 1 μm).

Table 4. Effect of the re-sintering treatment by hot uniaxial pressing on density on samples sintered at 1400°C for 2 h

Forging temperature (°C)	Axial strain (%)	Crosshead speed (μm min ⁻¹)	Relative density ^a ρ _s (%)	Relative density ^a ρ _{sf} (%)
1400	5	5	96	98
1400	10	5	96	98
1400	15	5	96	98
1400	10	20	96	98
1400	10	50	96	98
1300	10	5	96	98
1300	10	20	96	98
1300	10	50	96	98

^aρ_s ρ_{sf} are, respectively, the body density before and after re-sintering. ρ_{th} (5YSZ) = 6.03 g cm⁻³.

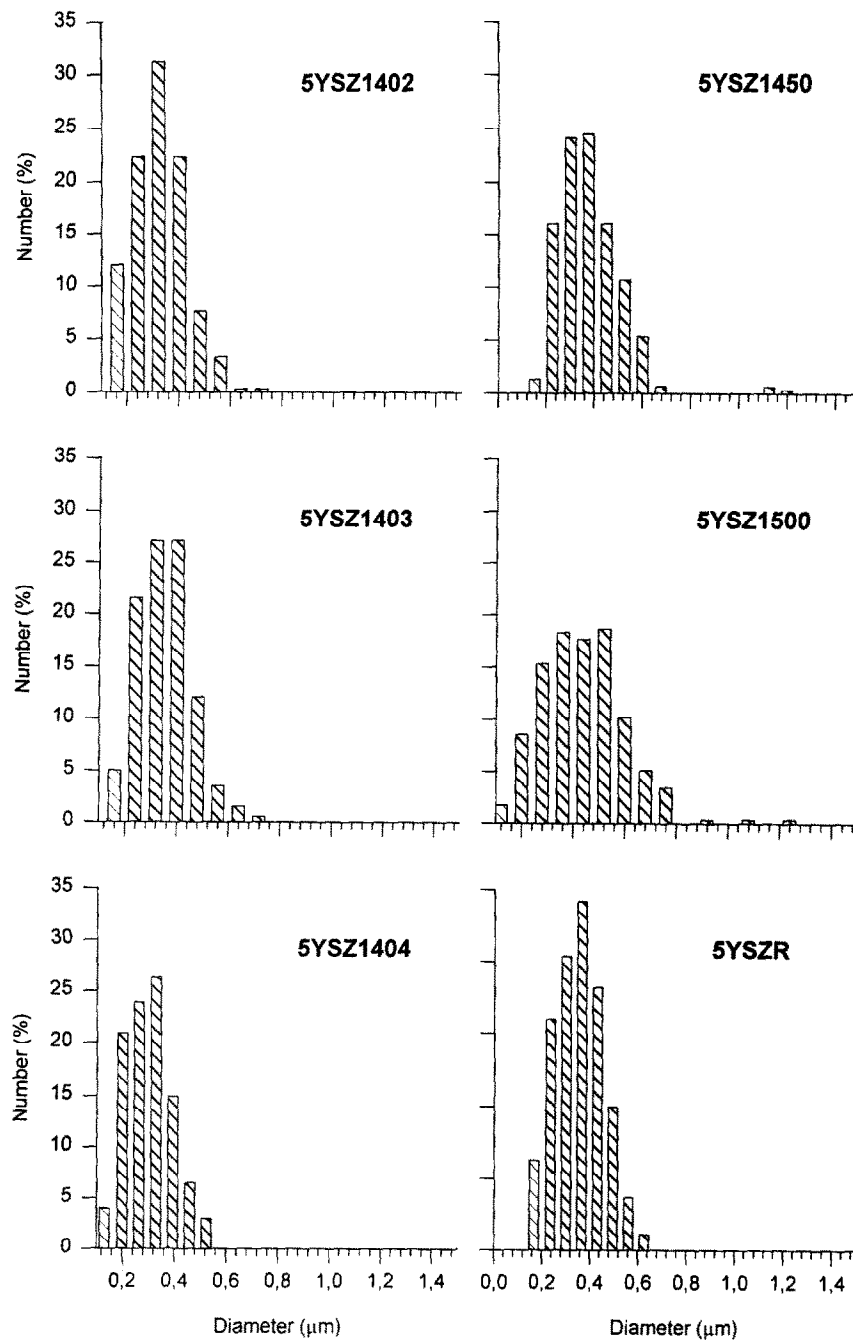


Fig. 10. Particle size distribution of sintered samples at: (a) 1400°C for 2 h; (b) 1400°C for 3 h; (c) 1400°C for 4 h; (d) 1450°C for 2 h; (e) 1500°C for 2 h; (f) 1400°C for 2 h and resintered at 1400°C.

Table 5. Refinement data, phase compositions (wt%), crystallite size and cell parameters obtained from 5YSZ samples according to the different heat treatments

Sample	Phase	X	a (nm)	b (nm)	c (nm)	$\gamma(^{\circ})$	wt%
5YSZ-1400	t-ZrO ₂	0.050	0.3604	—	0.5182	—	19.53
	t'-ZrO ₂	0.014	0.3627	—	0.5244	—	14.87
	m-ZrO ₂	0.022	0.5160	0.5209	0.5327	99.44	36.41
	c-ZrO ₂	0.078	0.5134	—	—	—	29.19
5YSZ-1550	t-ZrO ₂	0.058	0.3604	—	0.5181	—	61.89
	t'-ZrO ₂	0.071	0.3635	—	0.5353	—	3.14
	m-ZrO ₂	0.050	0.5159	0.5209	0.5327	99.44	13.05
	c-ZrO ₂	0.082	0.5133	—	—	—	21.92
5YSZ-1400R	t-ZrO ₂	0.050	0.3604	—	0.5182	—	15.52
	t'-ZrO ₂	0.014	0.3667	—	0.5244	—	10.77
	m-ZrO ₂	0.022	0.5160	0.5209	0.5327	99.44	46.53
	c-ZrO ₂	0.078	0.5134	—	—	—	27.58

3.2 Dilatometry

Figure 7 shows the linear shrinkage versus temperature and time for different heat-treatments. The codes are specified in Table 1. The curves reveal that sintering starts at 950°C, independently of the heating rate. In all the cases the shrinkage reaches about 30%, the heating rate and the sintering temperature do not influence the final density [Fig. 7(b)].

Considering different curves, from 1400°C on the samples do not shrink but those that have been scheduled to reach 1600°C begin to suffer thermal expansion. C4, scheduled until 1400°C, linearly shrinks and no completion of this process is

observed after 10 h dwell. The different shrinking rates values are caused by the variation of the heating rate [Fig. 7(a)]. Dilatometric data are confirmed by the measurement of the density of sintered pellets using Archimedes' method Table 1.

The sintering schedule employed in our samples was chosen after the dilatometric tests output as well as regarding the grain growth experimented for the samples for each particular sintering schedule. The best result was reached when the temperature was raised up to 1400°C, at a rate of 300°C h⁻¹ up to 1100°C and of 60°C h⁻¹ up to the sintering temperature, the samples were held at this temperature for 2, 3 or 4 h. No significant improvement of the final densities were observed for isothermal treatments longer than 2 h.

3.3 Characterization of the green bodies

Mercury porosimetry results (Fig. 8) show pore radii distribution is in the range 60-150 nm for all samples with a maximum between 80 and 100 nm. If the pore mean diameter is compared to crystallite diameter size obtained by SEM (Fig. 3), it can easily be noticed that the samples exhibit mainly intergranular porosity. In addition, a very small porosity is discerned for the samples with a pore radii larger than 10⁵ nm.

SEM micrographs of green bodies (Fig. 9) shows that they present a very uniform aspect indicating that the compaction process of powders is controlled by a crushing phenomenon of their agglomerates, since they do not stand after applying uniaxial pressure (75 MPa).

3.4 Characterization of the sintered bodies

Slight grain growth is observed in the samples sintered at 1400°C for 2, 3 or 4 h (referred as 5YSZ1400), with respect to the 5YSZ800 powders. No appreciable difference exists between them, the grain sizes of which ranging from 150 to 700 nm, Fig. 10. The micrographs in Fig. 11 show that the material consists of a distribution of small and

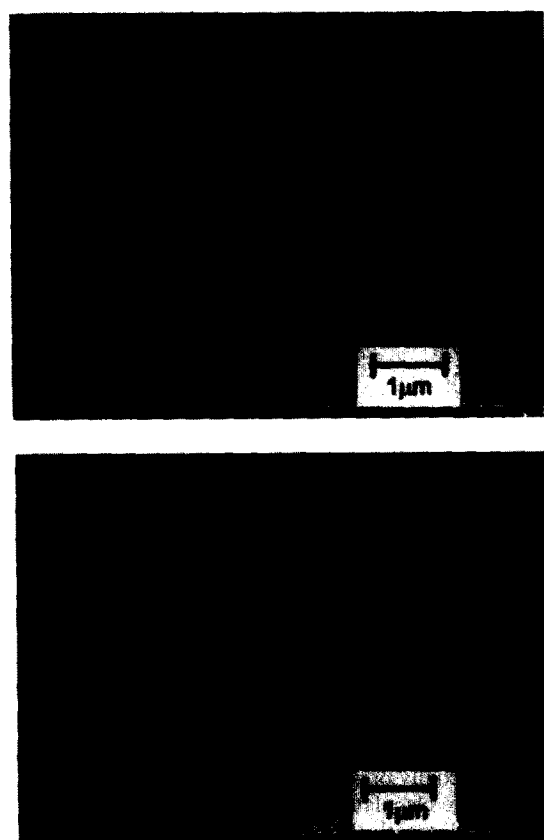


Fig. 11. Series of scanning electron micrographs showing polished and thermally etched surfaces sintered at 1400°C; (a) for 2 h; (b) for 4 h (bars = 1 μm).

monosized grains, 300-350 nm average diameter. A sintering temperature of 1450°C involves increasing the average grain size by 10%, exceeding more of them $> 0.3 \mu\text{m}$ that is the critical size required for the retention of the tetragonal structure¹⁸⁻²⁰ (Fig. 10). Increasing the sintering temperature from 1400 to 1600°C causes the average grain size to increase to 950 nm and the grain size distribution to broaden, with grains now ranging from 0.16 to $3.3 \mu\text{m}$ [Figs 11 and 12(a) and (b)]. Selected areas electron diffraction analyses of similar materials by

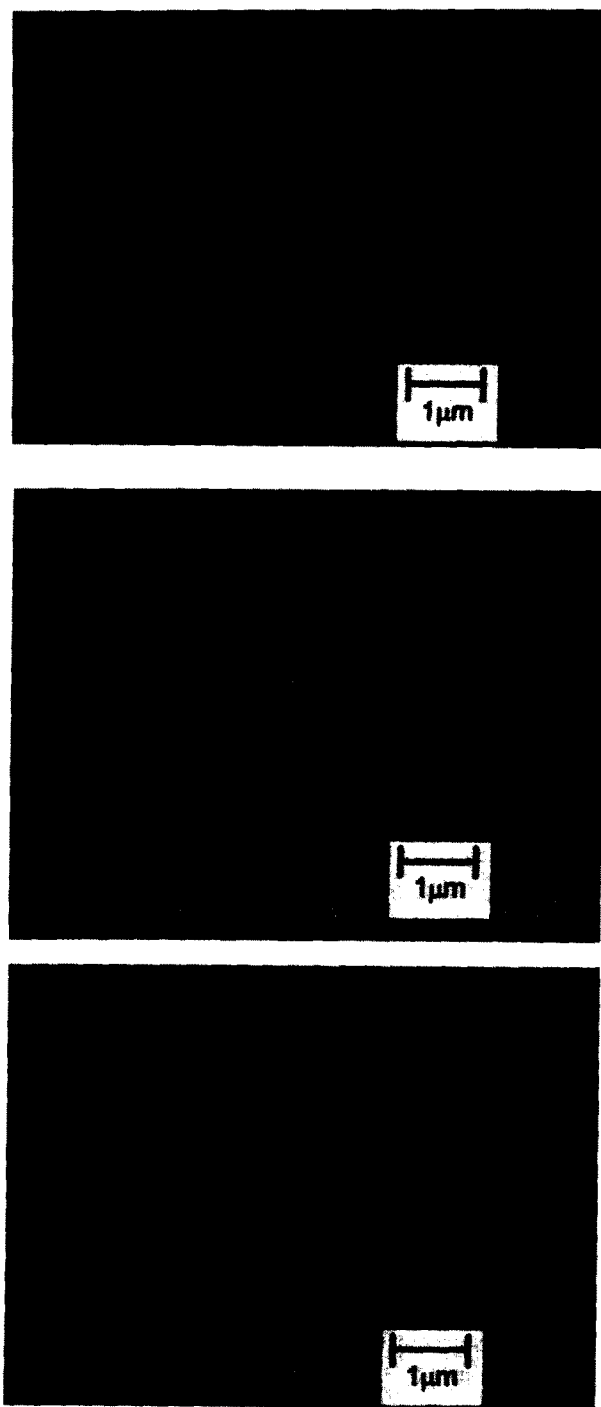


Fig. 12. Series of scanning electron micrographs showing polished and thermally etched surfaces; (a) sintered at 1500°C for 2 h, (b) sintered at 1600°C for 2 h and (c) sintered at 1400°C for 2 h and resintered at 1400°C under hot uniaxially pressure (bars = $1 \mu\text{m}$).

other investigators have shown that the larger grains have the cubic structure, whereas the smaller grains are tetragonal.²¹

Table 4 presents the detailed conditions and results of the resintering process under uniaxially pressure in the same order they were carried out. As can be seen, no significant variation in density is achieved after 5, 10 or 20% axial strains (at 1400°C and $5 \mu\text{m min}^{-1}$ crosshead speed); hence the rest of the experiments were performed deforming the samples to intermediate strain, 10%. Variation of the crosshead speed ($5-20 \mu\text{m}$) and working temperature (1300°C versus 1400°C) also yield similar values of densities in all cases.

No remarkable differences in grain size have been observed between pellets submitted to different thermo-mechanical treatment schedules. The

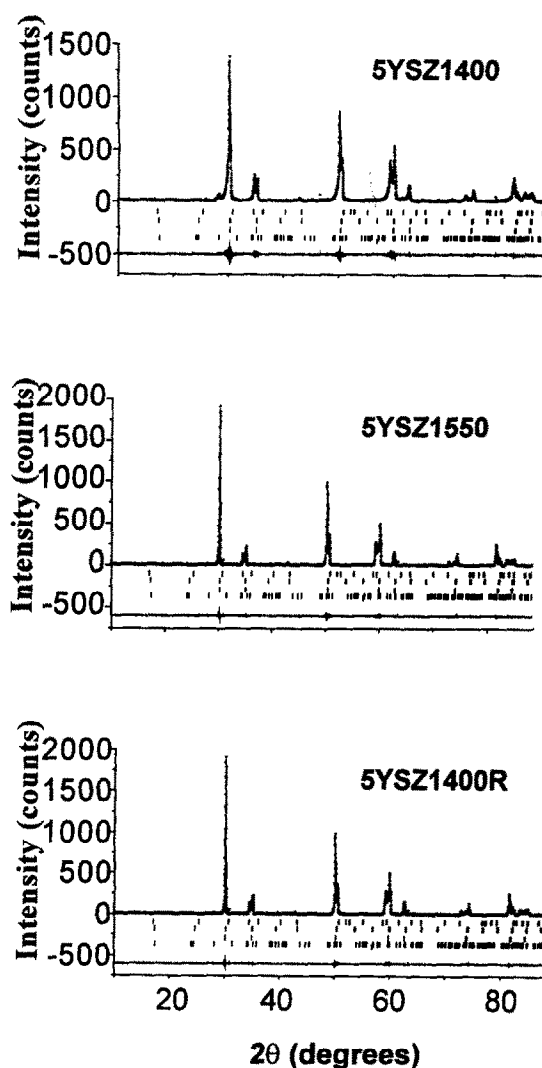


Fig. 13. Rietveld plots for diffraction data collected from 5YSZ sintered bodies at: (top) 1400°C for 2 h, (middle) 1500°C for 2 h, and (bottom) 1400°C for 2 h and resintered 1400°C under hot uniaxially pressure. The observed data are indicated by dots and the calculated pattern by the solid line overlying them. Bars underneath the pattern show the calculated Bragg-reflections corresponding to the different phases in the same order that they appear in the respective tables. The line at the bottom of the pattern is the difference between the observed and calculated profiles.

grain size distribution of compacts sintered at 1400°C does not change significantly after resintering [Figs 10, 11 and 12(c)], referred as 5YSZ1400R. No intragranular pores have been observed either in sintered or resintered samples.

Figure 13 shows the refining output plots indicating the difference between the calculated and experimental profiles, as well as the Bragg reflection of the phases assumed for the fitting corresponding at sintered samples at different heat-treatment. In all cases the best fits were obtained assuming all four phases were present. It is worth commenting that the patterns obtained before polishing did not show evidence of a monoclinic phase. The final values of the parameters and the percentage of each of the phases are listed in Table 5. Both monoclinic and cubic phases content diminish with increasing sintering temperature, but they increase with the resintering treatment. No free yttria traces were found.

4 Conclusions

5YSZ powders have been prepared from controlled hydrolysis of alkoxides. The powders after calcination at 600°C contain primary crystallites with an average particle diameter of 180 nm.

Sintering starts at 950°C, independently of the heating rate. In all cases the shrinkage reaches about 30%, the heating rate and the sintering temperature do not influence the final density. Green bodies present a very uniform aspect. The compaction process of powders is controlled by a crushing phenomenon of their agglomerates.

Slight grain growth is observed in the samples sintered at 1400°C, with respect to the 5YSZ800 powders. No appreciable difference exists between them, the grain sizes of which ranging from 200 to 400 nm. The samples sintered at 1400°C consists of a distribution of small and monosized grains, 300–350 nm average diameter. A 50°C increase of the sintering temperature represents that the critical size (0.3 μm) required for the retention of the tetragonal structure is overstepped by most of grains. Increasing the sintering temperature from 1400 to 1600°C causes the average grain size to increase three times with grains now ranging from 0.16 to 3.3 μm .

The sintering schedule that gave the smallest grain size (average grain size < 300 nm) was heating at 5° min⁻¹ up to 1100°C and then at 1°C min⁻¹ up to 1400°C holding this temperature for 2 h.

Resintering did not lead to a grain growth. It increases the density of the 5YSZ1400 from 96 to 98% by collapsing pores. Both monoclinic and

cubic phases increases with such a treatment. No remarkable differences in grain size have been observed between pellets submitted to different thermo-mechanical treatment schedules.

Acknowledgements

This work has been supported by the Spanish Government (CICYT Project No.MAT94-0120-C03), Junta de Andalucía (exp. No.6015). The authors are indebted to Professor Domínguez-Rodríguez from the Universidad de Sevilla (Spain), where the resintering experiments were carried out, to Mr José M^a Geraldía from the Universidad de Cádiz (Spain) for their co-operation concerning electron microscopy and to Mr Émile Gasque from the Université de Montpellier 2 (France) designing an appropriate die for dilatometry. SEM and XRD were performed at the Servicio de Ciencia y Tecnología de la Universidad de Cádiz, Spain.

References

1. Fegley, B. Jr and Barringer, E. A., Synthesis characterization and processing of monosized ceramic powders. In *Better Ceramics Through Chemistry*, Proceedings of the Materials Research Society Symposium, Vol. 32, ed. Brinker, C. J. Elsevier, New York, 1984, pp. 187–197.
2. Barringer, E. A. and Bowen, H. K., Formation, packing and sintering of monodispersed doped TiO₂ powders. *J. Am. Ceram. Soc.*, 1982, **65**, C 199-C 201.
3. Fegley, B., Barringer, E. A. and Bowen, H. K., Synthesis and characterization of monodispersed doped TiO₂ powders. *J. Am. Ceram. Soc.*, 1984, **67**, C 113-C 115.
4. Jiménez-Solís, C., Esquivias, L. and Prieto, C., Short-range order of yttria doped zirconia powders study by X-ray absorption (I). *J. Alloys and Compounds*, 1995, **228**, 188–194.
5. Esquivias, L., Barrera-Solano, C., Piñero, M. and Prieto, C., Short-range order of yttria doped zirconia powders study by X-ray absorption (II). *J. Alloys and Compounds*, 1996, **239**, 71–76.
6. Lange, F. F., Davis, B. I., and Wright, E., Processing related fracture origins: IV, Elimination of voids produce by organic inclusions. *J. Am. Ceram. Soc.*, 1986, **69** (1), 66–69.
7. Venkatachari, K. R. and Raj, R. Superplastic deformation of fine grained alumina. *J. Am. Ceram. Soc.*, 1986, **65**, (2), 336–341.
8. Venkatachari, K. R. and Raj, R. Enhancement of strength through sinter forging. *J. Am. Ceram. Soc.*, 1987, **70**, (7), 514–524.
9. Rodríguez, J., Anne, M. and Pannetirr, J., in A System for Time-Resolved Data Analysis (Powder Diffraction Pattern). Institute Laue-Langevin (ILL) Internal Report 87R014T, 1987.
10. Marquardt, D. W., An algorithm for least-squares structure estimation of nonlinear parameters. *J. Soc. Indust. Appl. Math.*, 1963, **11**, 431–441.
11. Rodríguez, J., Anne, M. and Pannetirr, J., in A System for Time-Resolved Data Analysis (Powder Diffraction Pattern), ILL Internal 87R014T, 1987.
12. Teufer, G., Crystal structure of tetragonal ZrO₂. *Act. Cryst.*, 1982, **15**, 1187.
13. Smith, D. K. and Newtik, H. W., Crystal structure of baddeleyite monoclinic ZrO₂. *Act. Cryst.*, 1965, **18**, 983–991.

14. Smith, D. K. and Cline, C. F., Verification of existence of cubic zirconia at high temperature. *J. Am. Ceram. Soc.*, 1962, **45**, 249–250.
15. Thompson, P. Cox, D. E. and Hasting, J. B., Rietveld refinement of Debye–Scherrer synchrotron X-ray data from Al_2O_3 . *J. Appl. Cryst.*, 1987, **20**, 79–83.
16. Hill, R. J., Data collection strategies: fitting the experiment to the need. In *The Rietveld Method.*, ed. Young, R. A. Oxford University Press, Oxford, 1995, p.95.
17. Ingel, R. P. and Lewis, D., Lattice parameters and density for Y_2O_3 -stabilized ZrO_2 . *J. Am. Ceram. Soc.*, 1981, **69**, 325–332.
18. Lange, F. F., Transformation toughening: Part 3, Experimental observations in the ZrO_2 – Y_2O_3 system. *J. Mater. Sci.*, 1982, **17**, 240–246.
19. Gupta, T. K., Lange, F. F. and Bechtold, J. H., Effect of stress-induced phase transformation on the properties of polycrystalline zirconia-containing tetragonal phase. *J. Mater. Sci.*, 1978, **13**, 1464–1470.
20. Green, D. J., Critical microstructure for microcracking in Al_2O_3 – ZrO_2 composites. *J. Amer. Ceram. Soc.*, 1982, **65** (12), 610–614.
21. Rühle, M., Claussen, N. and Heuer, A. H., Microstructural studies of Y_2O_3 -containing tetragonal ZrO_2 Polycrystals (Y-TZP). In *Advances in Ceramics, Vol. 12, Science and Technology of Zirconia II*, ed. Claussen, N., Rühle, M. and Heuer, A. H., American Ceramic Society, Columbus, OH, 1984, pp. 352–370.